Supporting information

No-wash Immunosensors Based on Superhydrophilic Covalent Organic Framework Nanosheets with Aggregation-Induced Emission for Detecting Carbohydrate Antigen 19-9

Yue Du, Meiling Ye, Wentao Xu, Yonghai Song* and Li Wang[a]*

Nanofiber Engineering Center of Jiangxi Province, National Engineering Research Center for Carbohydrate Synthesis, Key Lab of Fluorine and Silicon for Energy Materials and Chemistry of Ministry of Education, College of Chemistry and Materials of Jiangxi Normal University, 99 Ziyang Road, Nanchang 330022, China.

*Corresponding author: Tel/Fax: +86 0791 88120861. E-mail: lwang@jxnu.edu.cn.

Materials and Method

Reagents

2,5-dihydroxyterephthalaldehyde (Dha) and 2,2',2'',2'''-(ethene-1,1,2,2-tetrayltetrakis([1,1'-biphenyl]-4',4-diyl))tetraacetonitrile (ETBT) were purchased from Bide Pharmatech Co., Ltd. (Shanghai, China). 3,3',5,5'-tetramethyl-[1,1'-biphenyl]-4,4'-diamine (TMB), NaCl, arginine (Arg), tyrosine (Tyr), cysteine (Cys), glutamate (Glu) were obtained from Shanghai Aladdin Biochemical Technology Co., Ltd (Shanghai, China). Neuron-specific enolase (NSE), carcinoembryonic antigen (CEA), carcinoembryonic antigen 19-9 (CA19-9), anti-CA 19-9 mouse monoclonal antibody (coating, Ab_1), anti-CA 19-9 mouse monoclonal antibody (labeling, Ab_2) were purchased from Shenggong Bioengineering Co., Ltd (Shanghai, China). The human serum samples were obtained from Beijing Solarbio Science & Technology Co., Ltd. K_2PtCl_6, and NaOH were acquired from Innochem Co., Ltd (Beijing, China). Methanol and acetone were obtained from Fuchen Chemical Reagent Co., Ltd. (Tianjin, China). *o*-dichlorobenzene (*o*-DCB), n-butyl alcohol (*n*-BuOH), N,N-dimethylformamide (DMF), acetic acid (HAc) and tetrahydrofuran (THF) were purchased from Xilong Chemical Co., Ltd (Guangzhou, China). Bovine serum albumin (BSA) was purchased from Sperikon Life Science & Technology Co., Ltd. (Sichuan, China). 0.2 M phosphate buffer solution (PBS) was prepared by 0.2 M NaH_2PO_4 and 0.2 M Na_2HPO_4. All reagents are analytically pure and do not need to be purified again.

Instruments

The excitation and emission spectra in a solution were detected on Hitachi F-7000 fluorescence spectrophotometer. The emission spectra in solid state were detected on Edinburgh FLS980 fluorescence spectrophotometer. The solid-state UV-visible absorption spectra were recorded by Shimadzu UV-3600i ultraviolet spectrophotometer. Scanning electron microscopy (SEM) images were obtained using HITACHIS-3400N with an acceleration voltage of 15 KV. Transmission electron microscopy (TEM) images were obtained via JEOL JEM-2100 microscopes at an acceleration voltage of 200 KV. Atomic force microscopy (AFM) images were collected by Bruker Nano-scope V (MultiMode 8) with ScanAsyst mode under atmosphere. Fourier transform-infrared spectroscopy (FT-IR) was measured by Perkin-Elmer's 200 spectrometer. On the D/Max 2500 V/PC X-ray powder diffractometer, X-ray diffraction (XRD) data was collected with Cu K Kα radiation (λ=1.54056 Å, 40 kV, 200 mA). N_2 adsorption/desorption isotherm tests were carried out by Autosorb-iQ (Quantachrome, USA) under 77 K. The wetting state was determined from contact angle measurements through the Krüss drop shape analyzer (DSA100). X-ray photoelectron spectroscopy (XPS) analysis was obtained by an AXIS SUPRA spectrometer (shimadzu, Japan).

Experiment section

Preparation of 2D AIE-CON$_{ETBT-Dha}$

To prepare 2D AIE-CON$_{ETBT-Dha}$, 0.0396 g of ETBT (0.05 mmol) and 0.0166 g of Dha (0.1 mmol) were homogeneously dispersed in 1 mL *o*-dichlorobenzene (*o*-DCB) and 1 mL n-butyl alcohol (*n*-BuOH) with sonicating for 15 min at a 10 mL reactor until the solution was well mixed. Then 200 μL of 4 M NaOH was added and the reactor was heated at 120°C for 3 days. After that, the mixture was cooled to room temperature and collected by high-speed centrifugation at 10,000 rpm for 3 min, washed with tetrahydrofuran (THF) and N,N-dimethylformamide (DMF) until the supernatant was clear and transparent. Finally, a brown solid was obtained, which was dried under vacuum in an oven at 60°C for 12 h to obtain 2D AIE-CON$_{ETBT-Dha}$ with of yield of 94%.

Preparation of PtNPs/AIE-CON$_{ETBT-Dha}$

First, 20 mg 2D AIE-CON$_{ETBT-Dha}$ was dispersed in 10 mL methanol and fully dispersed by ultrasonic treatment for 15 min. Next, 2 mL ultrapure water containing 4 mg K_2PtCl_6 was added, and the solution was kept stirring for 12 h to ensure that K_2PtCl_6 was fully reacted with CON$_{ETBT-Dha}$. Subsequently, $NaBH_4$ (1 mL, 0.25 M) was added drop by drop, and the reaction was continued for 6 h to achieve the coating of PtNPs. After the reaction completed, the precipitated product was collected by centrifugation and washed 3 times with ethanol to remove the unreacted substance and solvent. Finally, the washed product was dried to obtain PtNPs/CON$_{ETBT-Dha}$.

Construction of Ab/PtNPs/AIE-CON$_{ETBT-Dha}$ probe

First, 6 mg of PtNPs/AIE-CON$_{ETBT-Dha}$ were ultrasonically dispersed in 2 mL of 0.2 M phosphate buffer solution (PBS, pH=7.0) for 20 min to form a homogeneous solution, and then 0.6 mL of 100 μg/mL Ab (V_{Ab1}:V_{Ab2}=1:1) was added. The reaction was incubated at 4°C for 24 h. Next, 1 mL of 1%

bovine serum albumin (BSA) was added to the reaction system and incubated for 1 h to block the non-specific active sites. After that, the Ab/PtNPs/AIE-$CON_{ETBT\text{-}Dha}$ was washed three times with PBS to remove unbound Ab and BSA. Finally, the complex re-dispersed in 1 mL of PBS.

Fluorescence test of CA 19-9

First, 30 μL of 5 mg/mL Ab/PtNPs/$CON_{ETBT\text{-}Dha}$ ("Ab" refers to a 1:1 mixture of two monoclonal antibodies (Ab_1 and Ab_2)) solution was mixed well with 10 μL of 0.2 M PBS (pH = 7.0). Then, different concentrations of CA 19-9 solution were added drop by drop and the final volume was 1000 μL adjusted by PBS. The mixed solution was incubated and reacted under the optimal condition. After incubation for 60 min, fluorescence of the solution was measured by fluorescence spectrometer at 365 nm excitation wavelength. In the selectivity assay, CA 19-9 was replaced by interfering substances at 10 times under the same experimental conditions to investigate the effect of the interfering substance on the fluorescence characteristics of the system, and to evaluate the selectivity of the no-wash fluorescence-on immunosensors.

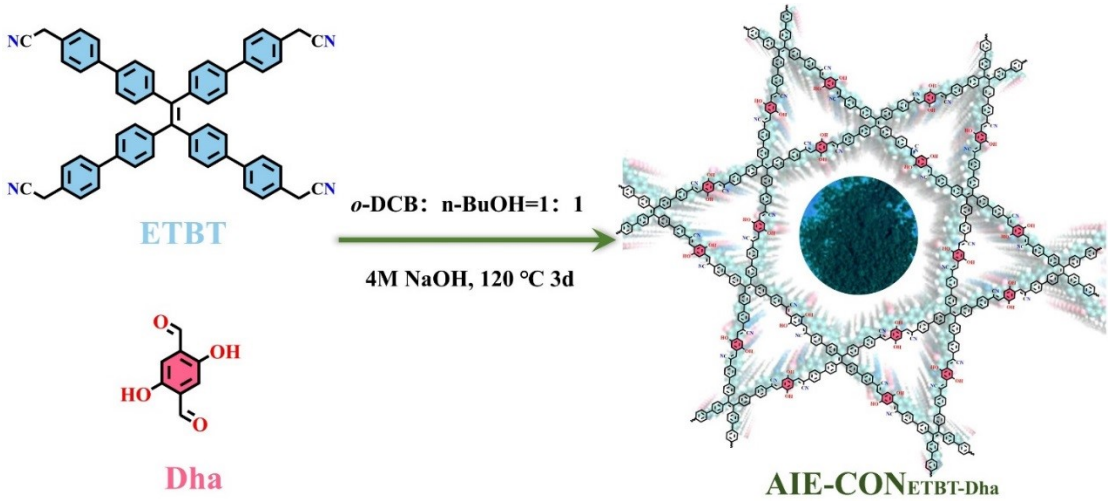

Fig. S1. Synthesis route of AIE-$CON_{ETBT\text{-}Dha}$.

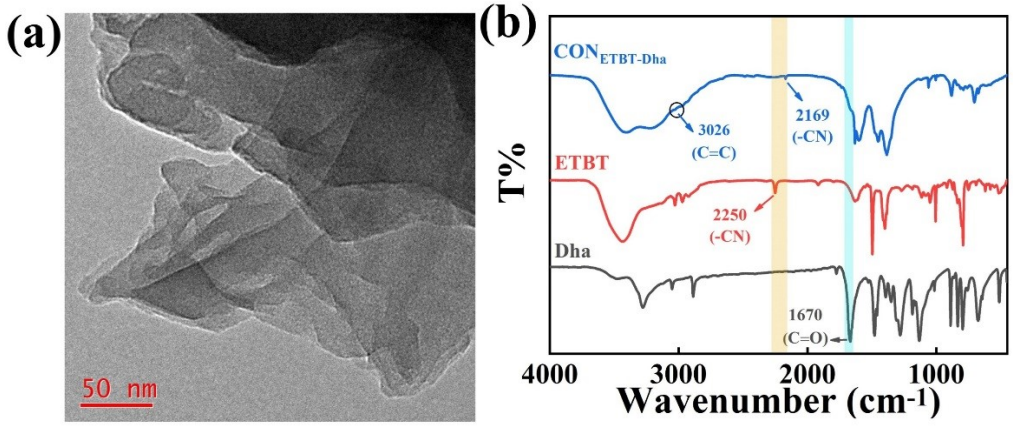

Fig. S2. (a) TEM image of AIE-$CON_{ETBT-Dha}$. (b) FTIR spectra of ETBT, Dha and AIE-$CON_{ETBT-Dha}$.

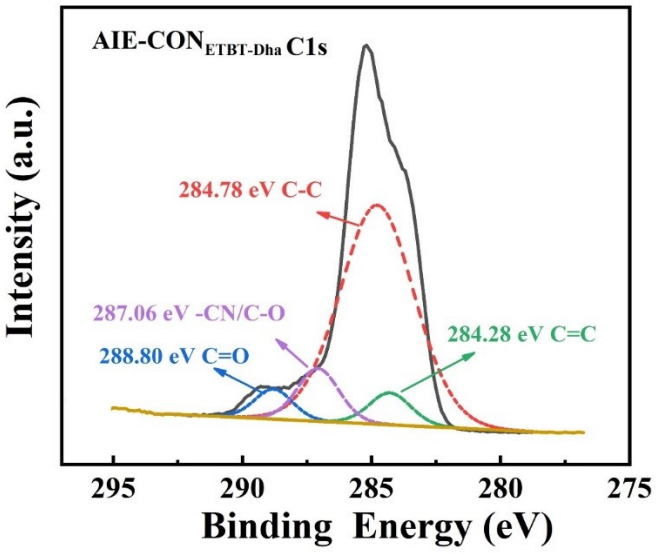

Fig. S3. C 1s XPS spectrum of AIE-CON$_{ETBT-Dha}$.

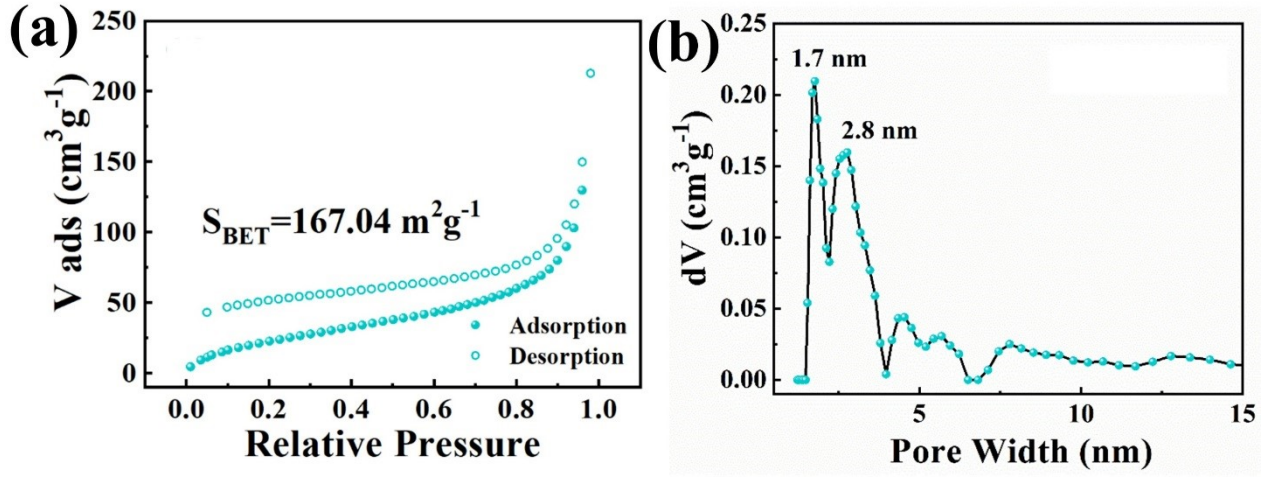

Fig. S4. (a) N_2 adsorption/desorption isotherm and (b) pore size distribution of AIE-$CON_{ETBT\text{-}Dha}$.

As shown in Fig. S3a, according to the Brunauer-Emmett-Teller (BET) model, the calculated surface area of AIE-$CON_{ETBT\text{-}Dha}$ was 167.04 m^2 g^{-1}. The nonlocal density functional theory (NLDFT) revealed the pore sizes of AIE-$CON_{ETBT\text{-}Dha}$ are 1.7 nm and 2.8 nm (Fig. S4b). The measured pore diameters are closer to the simulated values based on the AA stacking model.

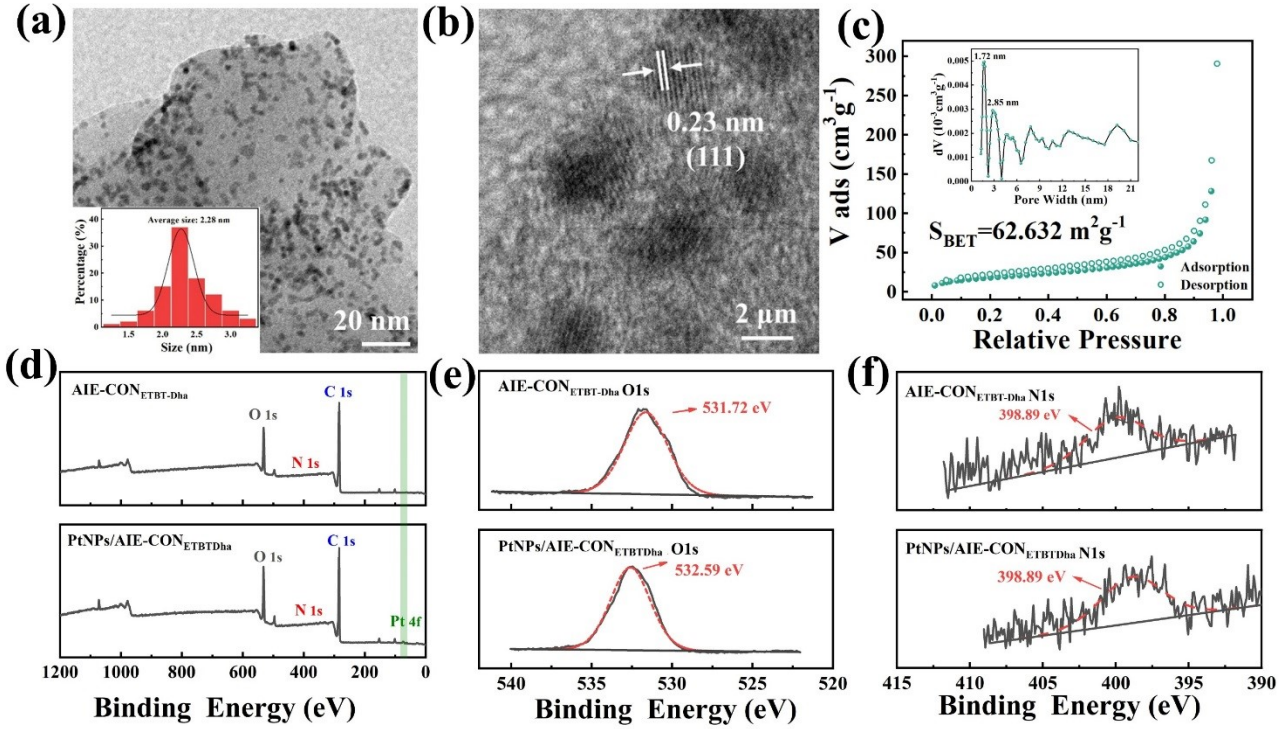

Fig. S5. (a) TEM image of PtNPs/AIE-CON$_{ETBT-Dha}$. Inset: size distribution of PtNPs. (b) HRTEM image of PtNPs/AIE-CON$_{ETBT-Dha}$. (c) N_2 adsorption/desorption isotherm of PtNPs/AIE-CON$_{ETBT-Dha}$. Inset: Pore size distribution of PtNPs/AIE-CON$_{ETBT-Dha}$. (d) XPS spectra of AIE-CON$_{ETBT-Dha}$ and PtNPs/AIE-CON$_{ETBT-Dha}$. XPS spectra of the survey O1s (e) and N1s (f) of AIE-CON$_{ETBT-Dha}$ and PtNPs/AIE-CON$_{ETBT-Dha}$.

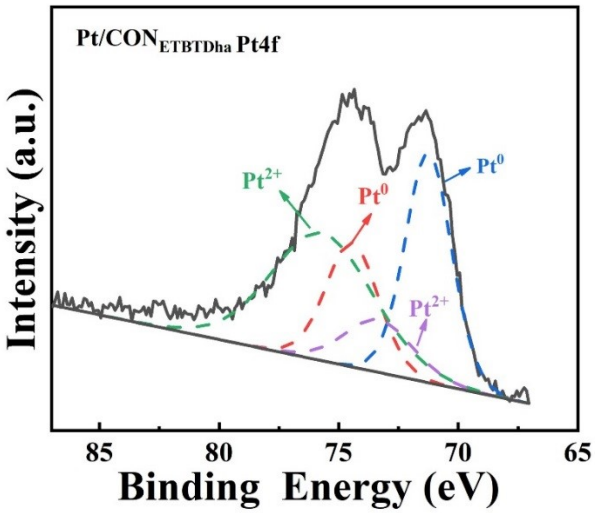

Fig. S6. Pt 4f XPS spectrum of PtNPs/AIE-CON$_{ETBT-Dha}$.

The spectrum of Pt 4f region consisted of a higher energy band (Pt $4f_{5/2}$) and a lower-energy band (Pt $4f_{7/2}$). The doublets can be divided into two pairs (Pt^0 and Pt^{2+} species): (1) Pt $4f_{5/2}$ (74.44 eV) and Pt $4f_{7/2}$ (71.25 eV), which can be assigned to Pt^0; (2) Pt $4f_{5/2}$ (75.70 eV) and Pt $4f_{7/2}$ (73.31 eV), which can be distributed to Pt^{2+}. The existence of Pt^{2+} species is due to the coordination of Pt^{2+} with O atom of OH.

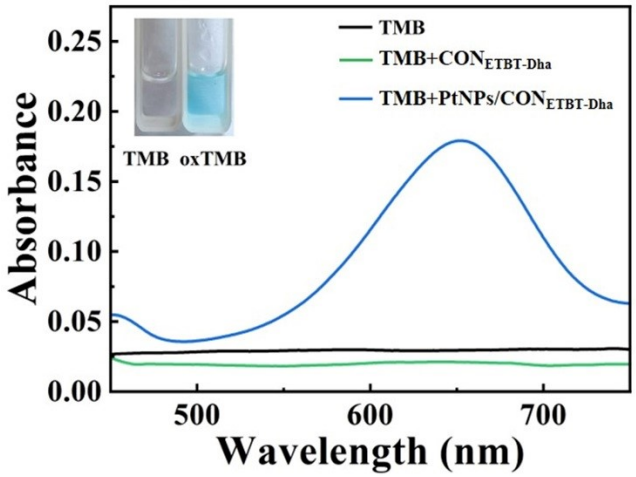

Fig. S7. UV-vis absorption spectra of TMB solution, TMB+AIE-CON$_{ETBT-Dha}$ solution and TMB+PtNPs/AIE-CON$_{ETBT-Dha}$ solution. Inset: Photos of reactions with TMB and oxTMB.

The PtNPs have outstanding oxidase-like activity and PtNPs/AIE-CON$_{ETBT-Dha}$ can catalyze the colorless 3,3′,5,5′-tetramethylbenzidine (TMB) to blue oxTMB.

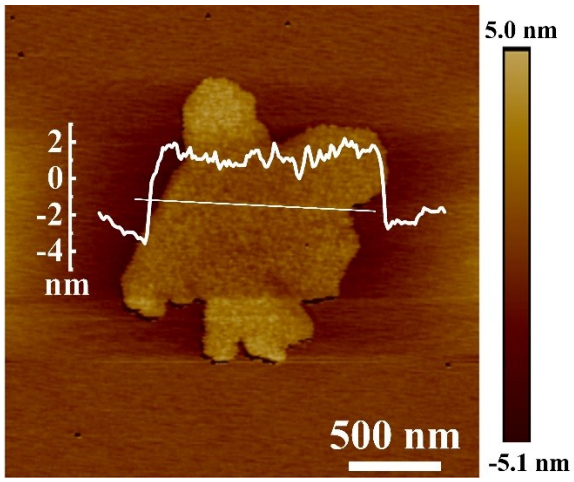

Fig. S8. AFM image of Ab/PtNPs/AIE-$CON_{ETBT\text{-}Dha}$.

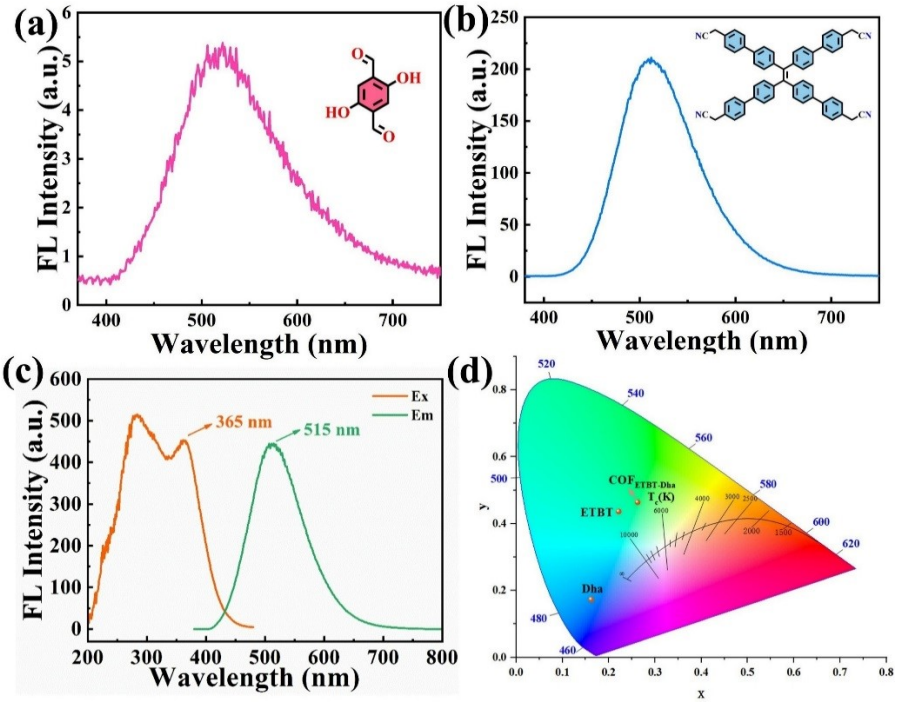

Fig. S9. (a) Fluorescence emission spectrum of Dha in aqueous solution. (b) Fluorescence emission spectrum of ETBT in aqueous solution. (c) Fluorescence excitation spectrum and emission spectrum of AIE-$CON_{ETBT\text{-}Dha}$ in aqueous solution. (d) CIE chromaticity diagram of ETBT, Dha and AIE-$CON_{ETBT\text{-}Dha}$.

As shown in Fig. S9c, the 2D AIE-$CON_{ETBT\text{-}Dha}$ in PBS (pH=7.0) showed an emission peak at 515 nm under 365 nm light excitation. Given the fluorescence intensity of Dha was extremely weak (Fig. S9a), the fluorescence of AIE-$CON_{ETBT\text{-}Dha}$ was mainly originated from ETBT (Fig. S9b). At the same time, the corresponding CIE chromaticity diagram of AIE-$CON_{ETBT\text{-}Dha}$ showed green light, close to that of ETBT (Fig. S9d).

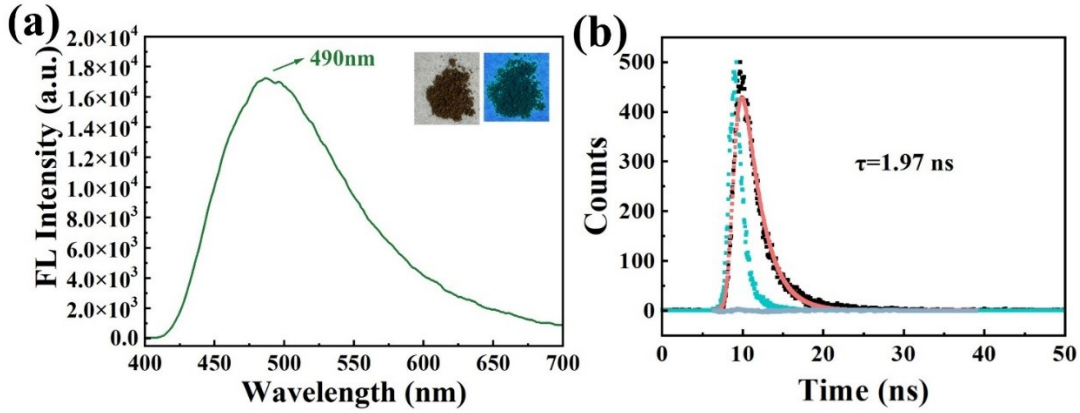

Fig. S10. (a) Emission spectrum of AIE-$CON_{ETBT\text{-}Dha}$ solid powder. Inset: photos of AIE-$CON_{ETBT\text{-}Dha}$ solid powder under visible light (left) and under UV 365 nm irradiation (right). (b) Fluorescence lifetime of AIE-$CON_{ETBT\text{-}Dha}$ in solid-state.

The fluorescence peak of solid-state AIE-$CON_{ETBT\text{-}Dha}$ was located at 490 nm (Fig. S10a). The AIE-$CON_{ETBT\text{-}Dha}$ solid powder is brown under sunlight and shows green fluorescence under ultraviolet light (inset of Fig. S10a). The fluorescence lifetime of solid-state AIE-$CON_{ETBT\text{-}Dha}$ is 1.97 ns (Fig. S10b).

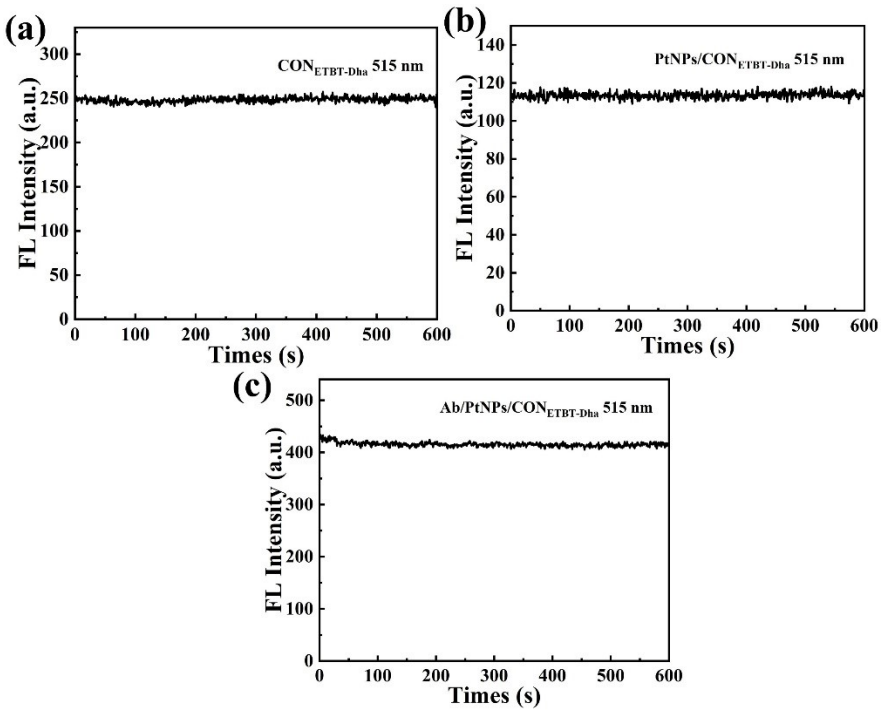

Fig. S11. Fluorescence stability of (a) AIE-CON$_{ETBT-Dha}$, (b) PtNPs/AIE-CON$_{ETBT-Dha}$ and (c) Ab/PtNPs/AIE-CON$_{ETBT-Dha}$.

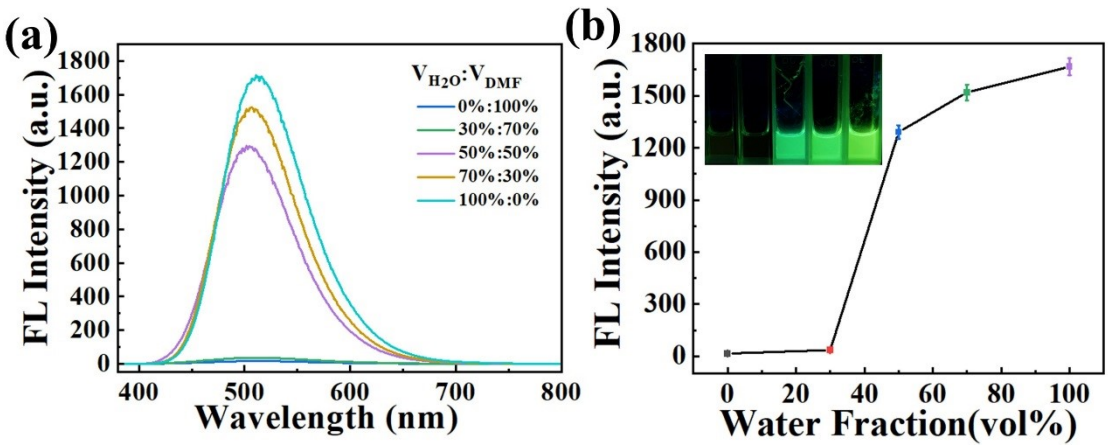

Fig. S12. (a) Fluorescence emission spectra of ETBT at different ratios of DMF with water. (b) Fluorescence emission intensity of ETBT at different ratios of DMF with water. Inset: pictures of ETBT at different ratio of DMF and water under UV 365 nm irradiation.

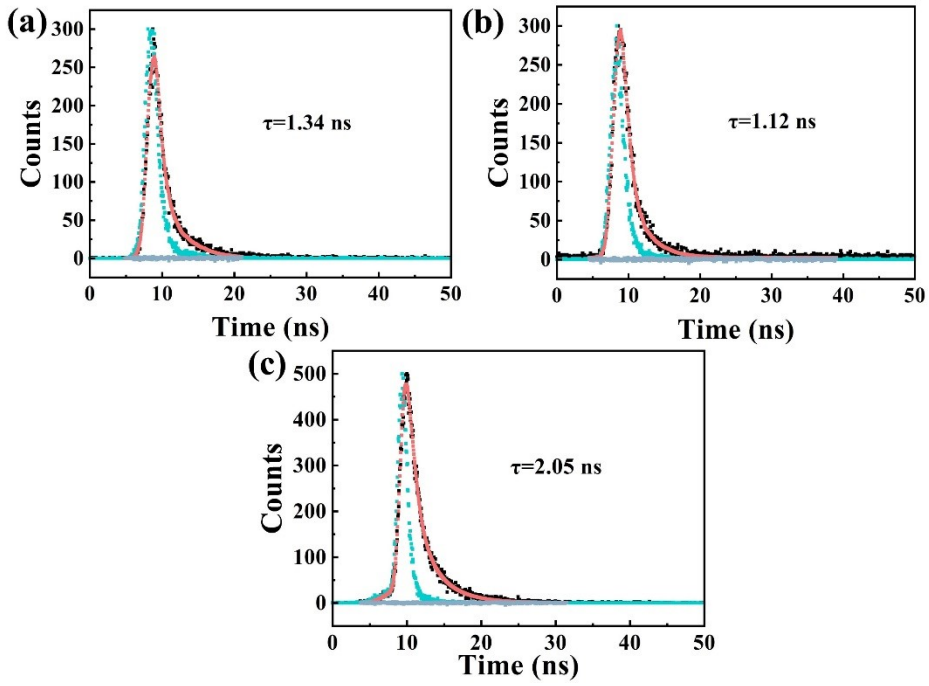

Fig. S13. Fluorescence lifetime of (a) AIE-$CON_{ETBT\text{-}Dha}$, (b) PtNPs/AIE-$CON_{ETBT\text{-}Dha}$ and (c) Ab/PtNPs/AIE-$CON_{ETBT\text{-}Dha}$ in a solution.

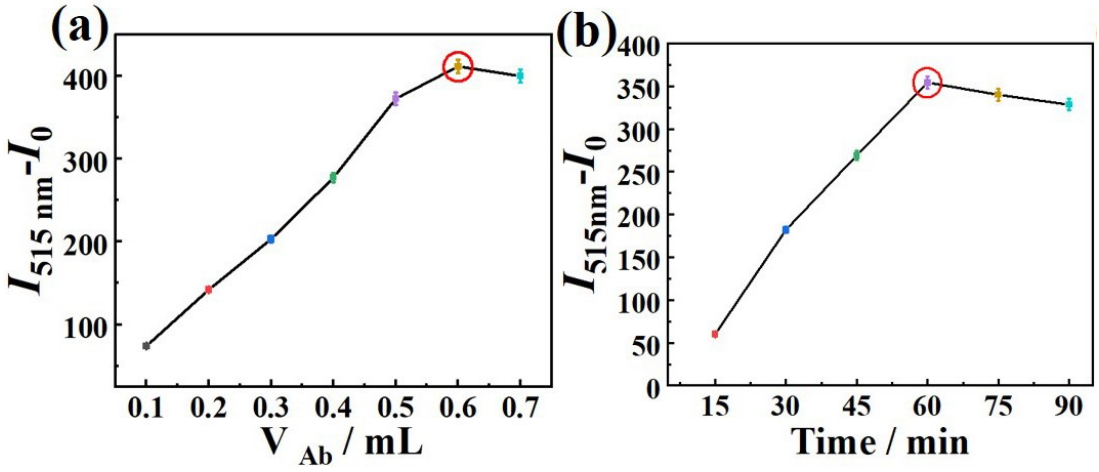

Fig. S14. (a) The effect of the volume of Ab solution (100 μg/mL) on the fluorescence response of 10.0 μU/mL CA 19-9 detected by PtNPs/AIE-$CON_{ETBT\text{-}Dha}$ (2.5 mg/mL). (b) The effect of incubation time on the fluorescence response of 10.0 μU/mL CA 19-9 detected by PtNPs/AIE-$CON_{ETBT\text{-}Dha}$ (2.5 mg/mL).

In order to acquire best sensing performance, the optimal experimental conditions during the construction of fluorescent immunosensor were explored. Effects of the incubation volume and time of Ab on the sensing performance were firstly explored. The experimental results showed that the optimal incubation volume of Ab solution was 0.6 mL when the concentration of PtNPs/AIE-$CON_{ETBT\text{-}Dha}$ was 2.5 mg/mL and the concentration of Ab (V_{Ab1}:V_{Ab2} = 1:1) was 100 μg/mL (Fig. S14a). Fig. S14b shows that the best incubation time was 60 min.

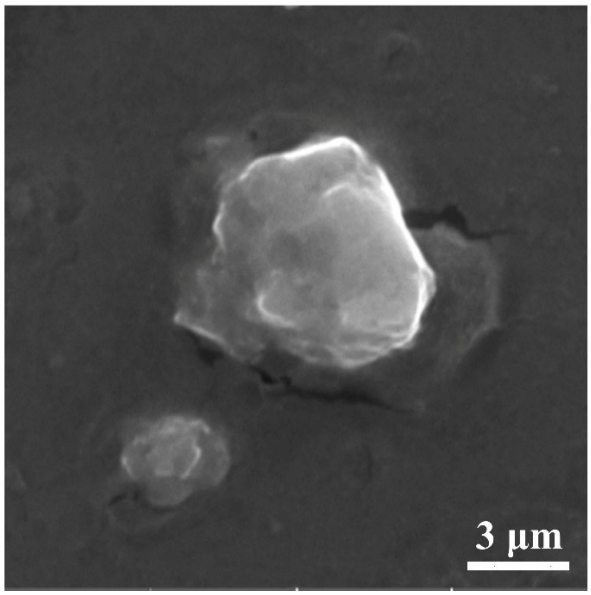

Fig. S15. SEM image of sandwich-type immunocomplex.

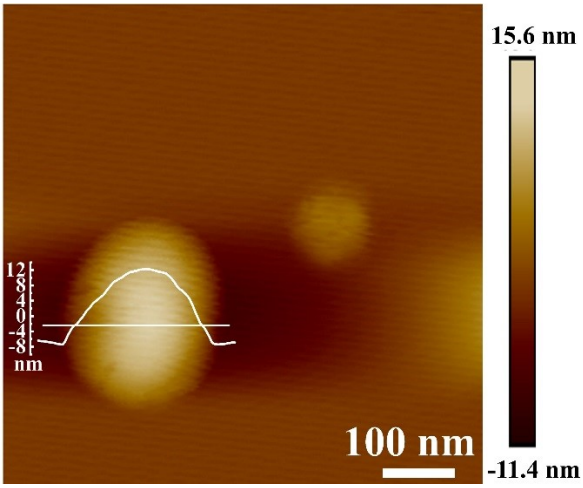

Fig. S16. AFM image of sandwich-type immunocomplex.

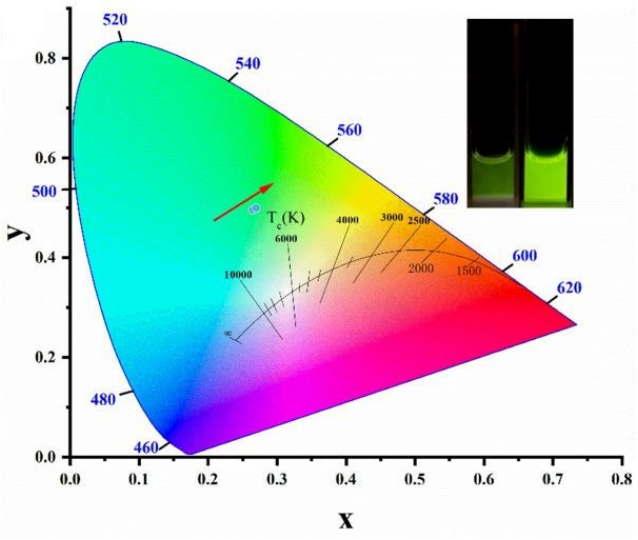

Fig. S17. CIE chromaticity diagram after adding different concentrations of CA 19-9. Inset: corresponding color change.

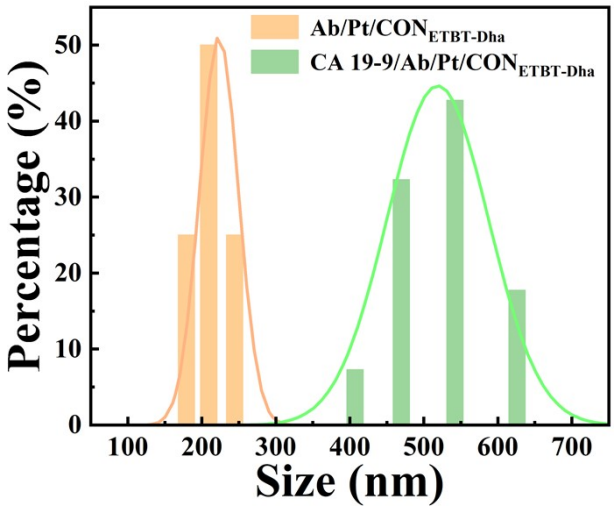

Fig. S18. The dynamic light scattering particle size of Ab/PtNPs/AIE-CON$_{ETBT-Dha}$ before and after CA 19-9 detection.

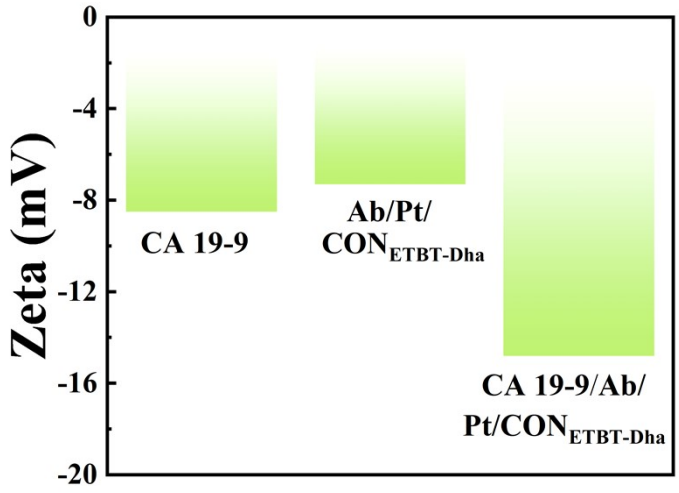

Fig. S19. Zeta potential of CA 19-9, Ab/PtNPs/AIE-$CON_{ETBT-Dha}$ and sandwich-type immunocomplex.

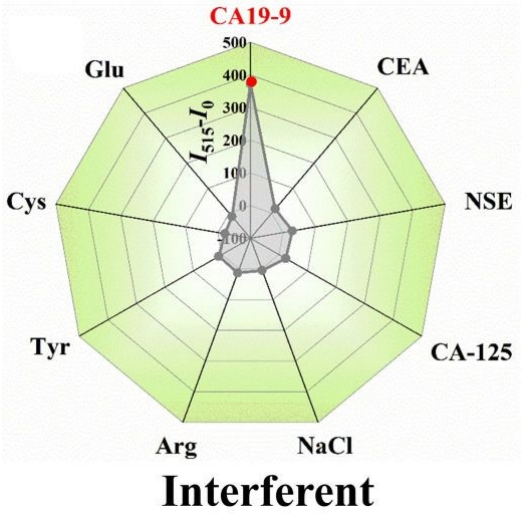

Fig. S20. Selectivity testing of CA 19-9 immunosensor.

To evaluate the selectivity of this immunosensor, interference tests were performed for several substances that may coexist with CA 19-9, including carcinoembryonic antigen (CEA), neuron-specific enolase (NSE), carbohydrate antigen 125 (CA 125), NaCl, arginine (Arg), tyrosine (Tyr), cysteine (Cys) and glutamate (Glu).

Table S1. Comparison of our present work with other methods for CA19-9 detection.

Materials	Method	Linear range ($U\ mL^{-1}$)	Detection limit ($U\ mL^{-1}$)	Sensitivity	Reference
ZnS@MSN-Glu	Electrochemistry	1×10^{-2} - 1×10^{2}	5×10^{-4}	1902	1
Fe_3O_4@TiO_2@AuNW nanocomposites	Surface-enhanced Raman scattering (SERS)	1×10^{-3} - 1×10^{3}	5.65×10^{-4}	2477.16	2
GCE/Au-In_2O_3/Ab_1/BSA/Ag/Cu_2S/CdSSe-Ab_2	Electrochemiluminescence	1×10^{-4} - 1×10^{2}	8×10^{-5}	1125.76	3
SiO2@Au-Ag Janus CJS	Surface-enhanced Raman scattering (SERS)	$3 \times 1\ 0^{-5}$ - 1×10^{4}	3.7×10^{-5}	2553	4
Ab/PtNPs/$CON_{TFBE-PDAN}$	Fluorescence	1×10^{-5} - 10	3.3×10^{-6}	136.51	5
Ag@EuW_{10}-PEI	Electrochemiluminescence	5×10^{-4} - 1×10^{2}	4×10^{-5}	1045	6
luminol-AgNPs@ZIF-67	Electrochemiluminescence	5×10^{-4} - 10	3.1×10^{-5}	1902	7

Pd@AuPt/MWCNT-NH_2-Bi-BiOI	Differential pulse voltammetry (DPV)	0.01 - 1.5 × 10^2	3.1 × 10^{-4}	20.83	8
CQDs/Au	Fluorescence	1 × 10^{-2} - 350	7 × 10^{-3}	2477.16	9
SiC@Ag	Surface-enhanced Raman scattering (SERS)	1 × 10^{-2}-1 × 10^3	1.3 × 10^{-3}	2454.7	10
Ab/PtNPs/AIE-$CON_{ETBT-Dha}$	Fluorescence	7.5 × 10^{-6}- 1 × 10^2	2.5 × 10^{-6}	2317.29	This work

ZnS@MSN-Glu: encapsulating glucose (Glu) within carrier mesoporous silica (MSN) with ZnS

Fe_3O_4@TiO_2@AuNW nanocomposites: Fe_3O_4@TiO_2@Au nanowires nanocomposites

GCE/Au-In_2O_3/Ab_1/BSA/Ag/Cu_2S/CdSSe-Ab_2: glassy carbon electrode/gold-doped diindium trioxide/CA19-9 antibody/Bovine serum albumin/Ag/Cu_2S/CdSSe-CA19-9 antibody

SiO_2@Au-Ag Janus CJS: SiO_2@Au-Ag Janus core-Janus satellite

Ab/PtNPs/$CON_{TFBE-PDAN}$: Anti-CA19-9 mouse monoclonal antibody/Anti-CA19-9 mouse monoclonal antibody/covalent organic framework nanosheet$_{4',4''',4'''',4''''''}$-(ethene-1,1,2,2-tetrayl)tetrakis(([1,1′-biphenyl]-4-carbaldehydE))-1,4-phenylenediacetonitrile

Ag@EuW_{10}-PEI: Ag@EuW_{10}-polyethyleneimine

luminol-AgNPs@ZIF-67: luminol-Ag nanoparticle@Zeolitic imidazolate frameworks-67

Pd@AuPt/MWCNT-NH_2-Bi-BiOI: Pd@AuPt/multi-walled carbon nanotubes -NH_2-Bismuth-bismuth iodide oxide

CQDs/Au: carbon quantum dots/gold

Table S2. Experimental results comparison of CA 19-9 in human serum samples using article method and ELISA method.

Added (U/mL)	Measured value by article method (U/mL)	Measured value by ELISA (U/mL)	Recovery by article method (U/mL)	Recovery by ELISA (%)	RSD by article method (%, n=3)	RSD by ELISA (%, n=3)
0.10	0.103	0.105	103.0	105.0	3.52	3.41
0.50	0.513	0.511	102.6	102.2	2.54	2.57
1.00	0.957	1.03	95.7	103.0	2.81	2.95

In order to verify the feasibility of Ab/PtNPs/AIE-CON$_{ETBT\text{-}Dha}$ in practical clinical applications, several recovery experiments have been performed on diluted actual human serum samples using the standard addition method. The serum sample was diluted 10-fold by PBS (pH=7) and added different concentrations (1.00 U/mL, 5.00 U/mL, 10.00 U/mL, respectively) of CA 19-9. The normal human serum samples were diluted 100-fold and employed as real samples using the standard addition method for analysis.

Supplementary References

1. G. Mo; X. He; D. Qin; S. Meng; Y. Wu and B. Deng, *Biosens. Bioelectron.,* 2021, **178**, 113024
2. Y. Tian; X. Li; F. Wang; C. Gu; Z. Zhao; H. Si and T. Jiang, *J. Hazard. Mater.*, 2021, **403**, 124009
3. Z. Gong; B. Lu; H. Wang; X. Ren; X. Liu; H. Ma; D. Wu; D. Fan and Q. Wei, *Anal. Chem.,* 2024, **96**, 1678-1685
4. H.L. Hao; J. Zhu; G.J. Weng; J.J. Li; Y.B. Guo and J.W. Zhao, *ACS Sensors,* 2024, **9**, 942-954
5. H. Wan; X. Wang; M. Ye; Q. Nie; Z. Zheng; L. Wang and Y. Song, *Anal. Chem.,* 2025, **97**, 10763-10771
6. D. Fan; B. Lu; A. Yan; Q. Su; H. Ma; X. Ren; L. Shi; D. Wu and Q. Wei, *Sens. Actuators: B Chem.,* 2025, **439**, 137863
7. G. Mo; X. He; D. Qin; S. Meng; Y. Wu and B. Deng, *Biosens. Bioelectron.,* 2021, **178**, 113024
8. S. Wu; H. Ma; L. Song; W. Zhong; Y. Gu; Y. Miao and Y. An, *Microchim. Acta,* 2025, **192**, 314
9. B. Li; Y. Li; C. Li; J. Yang; D. Liu; H. Wang; Rui Xu; Y. Zhang and Q. Wei, *Biosens. Bioelectron.,* 2023, **227**, 115180
10. L. Zhou; J. Zhou; Z. Feng; F. Wang; S. Xie and S. Bu, *Analyst,* 2016, **141**, 2534